

000
001
002
003
004
005
006
007
008
009
010
011
012
013
014
015
016
017
018
019
020
021
022
023
024
025
026
027
028
029
030
031
032
033
034
035
036
037
038
039
040
041
042
043
044
045
046
047
048
049
050
051
052
053

STIF: Learning Continuous Video Representation for Space-Time Super-Resolution

Anonymous CVPR submission

Paper ID 2977

Abstract

Videos typically record the streaming and continuous visual data as discrete consecutive frames. Since the storage cost is expensive for videos of high fidelity, most of them are stored in a relatively low resolution and frame rate. Recent works of Space-Time Video Super-Resolution (STVSR) are developed to incorporate temporal interpolation and spatial super-resolution in a unified framework. However, most of them only support a fixed up-sampling scale, which limits their flexibility and applications. In this work, instead of following the discrete representations, we propose a Space-Time Implicit Function (STIF) as a continuous representation for videos, and we show its applications for STVSR. The learned implicit neural representation can be decoded to videos of arbitrary spatial resolution and frame rate. We show that STIF achieves competitive performances with state-of-the-art STVSR methods on common up-sampling scales and significantly outperforms prior works on continuous and out-of-training-distribution scales.

1. Introduction

We observe the visual world in the form of streaming and continuous data. However, when we record such data with a video camera in a computer, it is often stored with limited spatial resolutions and temporal frame rates. Because of the high cost on recording and storing large time-scales of video data, oftentimes our computer vision system will need to process low-resolution and low frame rate videos. This introduces challenges in recognition systems such as video object detection [52], and we are still struggling at learning to recognize motion and actions from discrete frames [4, 12]. When presenting the video back to humans (e.g., on a TV), it is essential to visualize it in high resolution and high frame rate for user experience. How to recover the low resolution video back to high resolution in space and time becomes an important problem and the first step for many downstream applications.

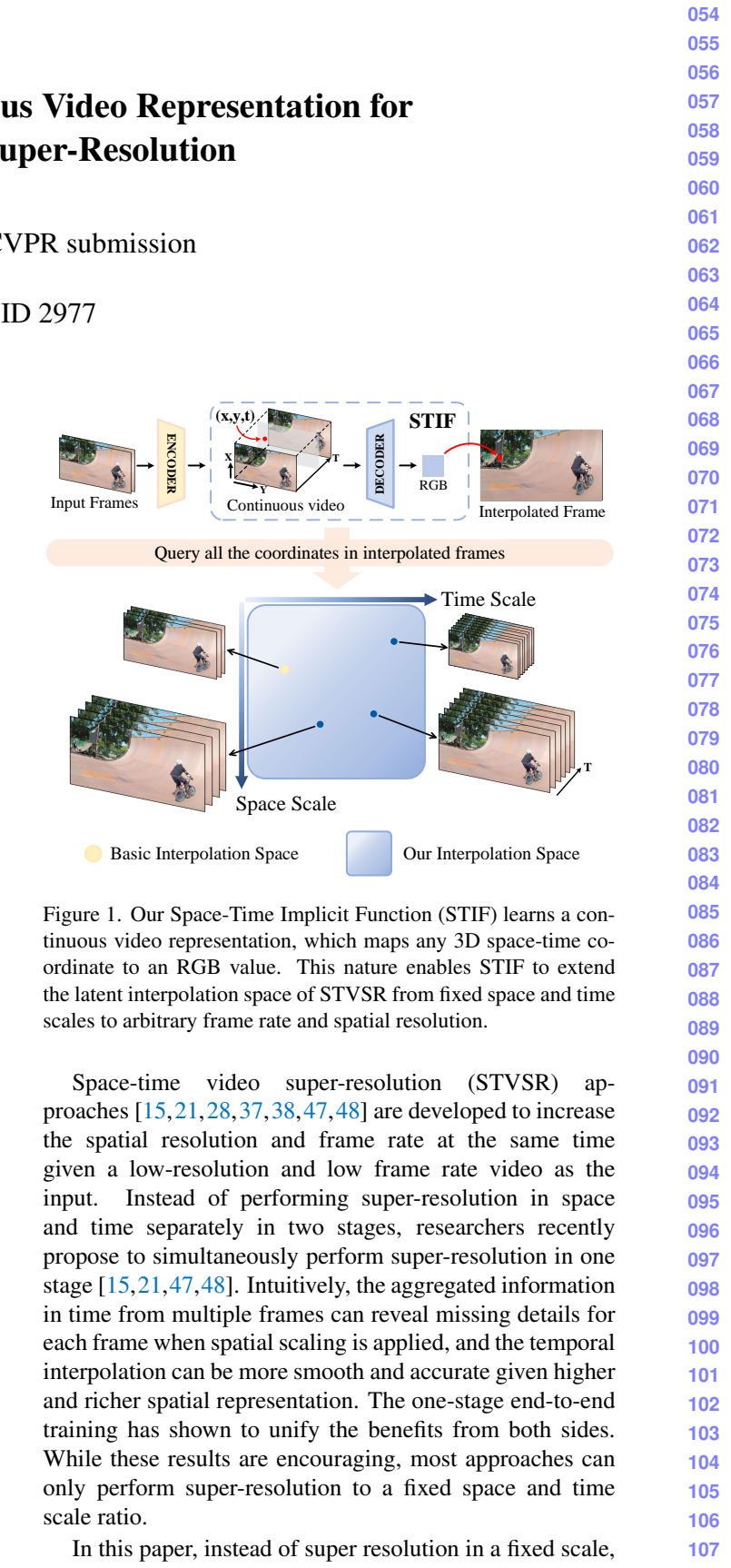


Figure 1. Our Space-Time Implicit Function (STIF) learns a continuous video representation, which maps any 3D space-time coordinate to an RGB value. This nature enables STIF to extend the latent interpolation space of STVSR from fixed space and time scales to arbitrary frame rate and spatial resolution.

Space-time video super-resolution (STVSR) approaches [15, 21, 28, 37, 38, 47, 48] are developed to increase the spatial resolution and frame rate at the same time given a low-resolution and low frame rate video as the input. Instead of performing super-resolution in space and time separately in two stages, researchers recently propose to simultaneously perform super-resolution in one stage [15, 21, 47, 48]. Intuitively, the aggregated information in time from multiple frames can reveal missing details for each frame when spatial scaling is applied, and the temporal interpolation can be more smooth and accurate given higher and richer spatial representation. The one-stage end-to-end training has shown to unify the benefits from both sides. While these results are encouraging, most approaches can only perform super-resolution to a fixed space and time scale ratio.

In this paper, instead of super resolution in a fixed scale,

108 we propose to learn a continuous video representation,
109 which allows to sample and interpolate the video frames
110 in arbitrary frame rate and spatial resolution at the same
111 time. Our key idea is to learn a neural implicit function,
112 which takes a space-time coordinate as input, and outputs
113 the corresponding RGB value. Since we can sample the
114 coordinate continuously, the video can be decoded in any
115 spatial resolution and frame rate. Our work is inspired by
116 recent progress on implicit functions for 3D shape represen-
117 tations [10, 13, 14, 26] and image representations with Local
118 Implicit Image Functions (LIIIF) using a ConvNet [7]. Dif-
119 ferent from images, where interpolation in space is based on
120 the gradients between pixels, pixel gradients across frames
121 with low frame rates are hard to compute. The network will
122 need to understand the motion of the pixels and objects to
123 perform interpolation, which is hard to model by 2D or 3D
124 convolutions alone.

125 We propose a novel Space-Time Implicit Function
126 (STIF) for continuous video representation. In the STVSR
127 task, two low-resolution image frames are concatenated and
128 forwarded to an encoder which generates a feature map with
129 spatial dimensions. STIF then defines a continuous video
130 representation over the generated feature map. It first uses a
131 spatial implicit function module to learn a continuous spa-
132 tial feature domain, from which a high-resolution image
133 feature is sampled according to all query coordinates. In-
134 stead of using convolutional operations to perform tempo-
135 ral interpolation, we design the temporal implicit function
136 module to first output a motion flow field given the high-
137 resolution feature and the sampling time as inputs. This
138 flow field will be applied back to warp the high-resolution
139 feature which will be decoded to the target video frame.
140 Since all the operations are differentiable, we can learn the
141 motion in feature level end-to-end without any extra su-
142 pervision besides the reconstruction error. To summarize,
143 given the input frames, an encoder generates a feature map,
144 which can be then decoded by STIF to arbitrary spatial res-
145 olution and frame rate.

146 In our experiments, we demonstrate that STIF can not
147 only represent video in arbitrary space and time resolu-
148 tions on the scales within the training distributions, but
149 also extrapolate to out-of-distribution frame rates and spa-
150 tial resolutions. Given the learned continuous function,
151 instead of decoding the whole video each time, it allows the
152 flexibility to decode only a certain region and time scale
153 when needed. We conduct experiments with Vid4 [23], Go-
154 Pro [29] and Adobe240 [41] datasets. We demonstrate that
155 STIF achieves competitive performances with state-of-the-
156 art STVSR methods on in-distribution spatial and temporal
157 scales and significantly outperforms other methods on out-
158 of-distribution scales.

159 We highlight our main contributions as follows:
160

- We propose a novel Space-Time Implicit Function as a

162 continuous video representation.

- The proposed approach allows for representing videos
163 in arbitrary space and time resolution efficiently with
164 one single network.
- STIF achieves out-of-distribution generalization and
165 outperforms baselines by a large margin.

2. Related Work

Implicit neural representation. Implicit neural represen-
171 tations have been demonstrated as compact yet powerful
172 continuous representations for various tasks, including 3D
173 reconstruction [10, 13, 14, 26] and generation [5, 11, 36].
174 These representations typically represent signals as a neu-
175 ral function that maps coordinates to signed distance [34],
176 occupancy [8, 24], or density and RGB values in a neu-
177 ral radiance field (NeRF [27]). Recent works also show
178 promising results of applying this idea for modeling 2D im-
179 ages [1, 7, 20, 40]. Our continuous video representation is
180 inspired by this rapidly growing field and has specific de-
181 signs for videos, where a learnable flow can exploit the cor-
182 respondences in video frames with inductive bias.

Video frame interpolation. Video frame interpolation
183 (VFI) aims to synthesize unseen frames between the in-
184 put video frames. Meyer *et al.* [25] proposed a phase-
185 based method where information across levels of a multi-
186 scale pyramid is combined for the synthesis of interpolated
187 frames. Niklaus *et al.* [32, 33] introduced a series of kernel-
188 based VFI algorithms in which they took pixel synthesis
189 for the target frame as local convolution over input frames.
190 Optical flow based VFI methods [2, 18, 30, 31, 49, 50] uti-
191 lized optical flow prediction networks (*e.g.* PWC-Net [42])
192 to compute bidirectional flows between input frames, which
193 served as the guidance for new frame synthesis. Additional
194 information including occlusion masks [18, 50], depth
195 maps [2], and cycle consistency [35] were also incorporated
196 in the models for better performances.

Video super-resolution. Video super-resolution (VSR)
197 aims at increasing the spatial resolutions of low-resolution
198 videos. Earlier approaches [3, 43, 50] were typically built
199 on the sliding-window framework, where they predicted
200 optical flows between input frames and performed spatial
201 warping for explicit feature alignment. Later on, implicit
202 alignment started a new trend in this task [6, 17, 19, 44, 45].
203 For instance, TDAN [44] adopts deformable convolutions
204 (DCNs) [9, 51] to align different input frames at feature lev-
205 els. EDVR [45] further extends DCNs to a multi-scale fash-
206 ion for more accurate alignment. Kelvin *et al.* introduced
207 BasicVSR [6], in which they analyzed basic components
208 for VSR models and suggested a bidirectional propagation
209 scheme to maximize the gathered information from input
210 frames.

Space-time video super-resolution The target of Space-
211 time video super-resolution (STVSR) is to simultaneously

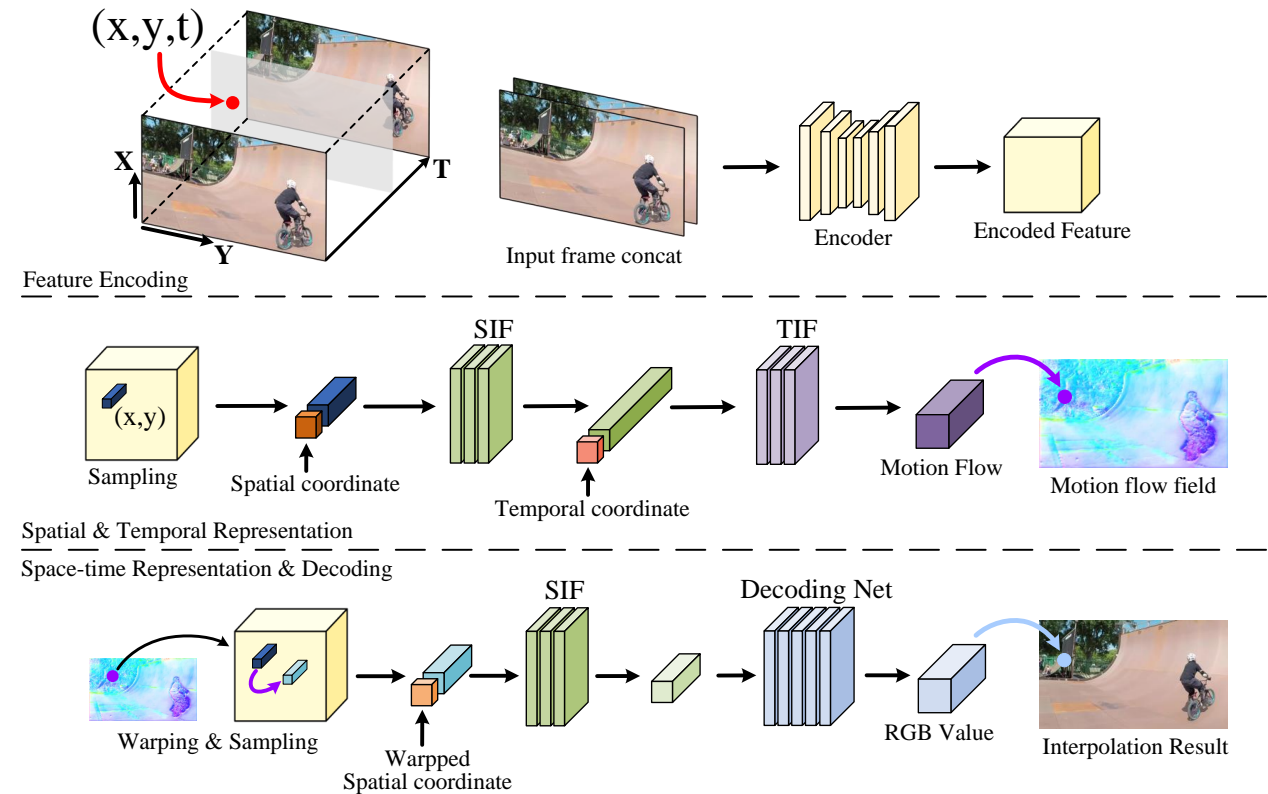


Figure 2. **A continuous video representation defined by Space-Time Implicit Function (STIF).** Two input frames are concatenated and encoded as a discrete feature map. Based on the feature, a 3D space-time coordinate is first decoded to a motion flow vector by a Spatial Implicit Function (SIF) and a Temporal Implicit Function (TIF). We then sample a new feature vector by warping according to the motion flow, and decode it as the RGB prediction of the query coordinate using a neural network. We omit the multi-scale feature aggregation part in this figure.

increase the spatial and temporal resolutions of the given low-resolution low frame rate videos. Shechtman *et al.* [38] tackled this problem by combining information from multiple input video sequences and applying a directional space-time regularization. Mudenagudi *et al.* [28] proposed a unified framework for STVSR in which videos are modeled as Markov random fields, and the maximum a posteriori estimates are taken as final solutions. Shahar *et al.* [37] introduced an effective space-time patch recurrence prior for STVSR. Recently, with the advances in deep learning, researchers started to employ powerful convolutional neural networks to address the task [15, 21, 47, 48]. Xiang *et al.* [47] proposed a unified neural network for synthesizing the feature of the missing frame and used a deformable ConvLSTM to align and aggregate extracted temporal information for reconstruction. STARNet [15] leveraged mutually informative relationships between time and space with the assistance of additional optical flow inputs. TMNet [48] proposed a temporal modulation block to modulate deformable convolution kernels for supporting frame interpolation at arbitrary time instances. All these STVSR

methods are designed to perform super-resolution on a specific up-sampling space scale defined before training, and some of them [15, 47] can only infer intermediate frames at pre-defined times. Therefore, the application scopes of these methods are limited. Our STIF is proposed to learn a continuous video representation that supports frame interpolation at arbitrary spatial resolution and frame rate. STIF is more flexible during the application and can be employed in more circumstances, such as non-uniform interpolation and video zoom-in in local regions.

3. Space-Time Implicit Function

Given a video with limited spatial resolution and frame rate, our goal is to find a continuous representation for the video. The representation interprets arbitrary space-time coordinate (x_s, x_t) into RGB values. To this end, we introduce the Space-Time Implicit Function (STIF), which produces continuous video representations of all videos. It is parameterized by multi-layer perceptrons (MLPs) and takes the form

$$s = f_\theta(x_s, x_t, \mathcal{V}) \quad (1)$$

324 where f_θ is the proposed space-time implicit function, \mathcal{V} is
 325 the given video, x_s is the 2D spatial coordinate, x_t is the
 326 temporal coordinate, and s is the predicted RGB value. In
 327 order to learn such neural implicit representation, we pro-
 328 pose to decouple space and time and adopt two implicit
 329 functions to represent them separately.
 330

331 Figure 2 illustrates an overview of our model. Given
 332 a space-time coordinate (x_s, x_t) and the feature extracted
 333 from input frames by an encoder, a spatial implicit function
 334 (SIF) is first utilized to decode the spatial coordinate
 335 x_s and output a corresponding feature vector (Sec. 3.1). The
 336 feature is then forwarded to the temporal implicit function
 337 (TIF) for the motion flow at the query coordinate (Sec. 3.2).
 338 The flow is applied back to warp the continuous feature de-
 339 fined by SIF for a new feature vector (Sec. 3.3) which is
 340 finally decoded to the target RGB value (Sec. 3.4).

341 3.1. Continuous Spatial Representation

342 Inspired by LIIF [7], we use a neural implicit function for
 343 learning a continuous spatial representation. The implicit
 344 function converts the discrete encoded feature map to a con-
 345 tinuous feature domain that decodes arbitrary 2D spatial co-
 346 ordinate into a corresponding feature vector. Specifically,
 347 the feature vectors generated by the encoder are evenly dis-
 348 tributed in the 2D space. We sample the feature vector (the
 349 dark blue cuboid in Fig 2) nearest to the queried spatial
 350 coordinate x_s , concatenate it with the relative position in-
 351 formation between query coordinate and feature vector, and
 352 input them into the Spatial Implicit Function (SIF) f_s to out-
 353 put the continuous feature at x_s (the green cuboid in Fig 2).
 354 This process could be expressed as
 355

$$356 \quad 357 \quad \mathcal{F}_s(x_s) = f_s(z^*, x_s - v^*) \quad (2)$$

358 where \mathcal{F}_s is the continuous feature domain defined by SIF,
 359 z^* is the feature vector nearest to the query coordinate x_s
 360 and v^* is the spatial coordinate of the feature vector z^* .
 361

362 The main difference between LIIF and SIF is that LIIF
 363 is proposed for continuous image representation, while SIF
 364 defines a continuous feature domain, which is supposed to
 365 be further utilized for modeling temporal information in
 366 videos.
 367

368 3.2. Continuous Temporal Representation

369 The proposed SIF defines a new continuous feature do-
 370 main in 2D space. Our next step is to learn the continuous
 371 temporal representation and extend the feature domain from
 372 2D space to 3D space and time, which can be achieved by
 373 decoding the temporal coordinate x_t . Directly generating
 374 the target decoded feature by a network can be fairly diffi-
 375 cult, as the network has to learn not only the motion patterns
 376 between input frames but also the context information. In-
 377 stead, we propose to learn a continuous motion flow field

378 for temporal representation. We introduce a temporal im-
 379 plicit function (TIF) to produce the motion flow.
 380

381 Given a 3D space-time coordinate (x_s, x_t) and input
 382 frames I_0 and I_1 , the goal of TIF is to learn a mapping from
 383 the coordinate to a motion flow
 384

$$385 \quad 386 \quad \mathcal{M}(x_s, x_t) = f_t(x_s, x_t, I_0, I_1) \quad (3)$$

387 where \mathcal{M} is the continuous motion flow field and f_t is the
 388 temporal implicit function. Benefiting from the 2D contin-
 389 uous feature domain provided by SIF, we could replace the
 390 two input frames and the spatial coordinate x_s in input pa-
 391 rameters of TIF with the continuous feature at x_s . Thus the
 392 equation could be written as
 393

$$394 \quad 395 \quad \mathcal{M}(x_s, x_t) = f_t(x_t, \mathcal{F}_s(x_s)) \quad (4)$$

396 where $\mathcal{F}_s(x_s)$ is the feature domain defined in Eq 2.
 397

398 In practice, we set the output of TIF as the combina-
 399 tion of two motion flows. Based on our observation, TIF
 400 would implicitly learn bi-directional flows under such set-
 401 ting, which could be interpreted as correspondences be-
 402 tween the target frame and two input frames.
 403

404 3.3. Space-Time Continuous Representation

405 With two continuous representations for space and time,
 406 we aim at combining them into a unified space-time contin-
 407 uous representation. Starting from a space-time coordinate
 408 (x_s, x_t) , we first use SIF to predict the continuous feature
 409 at x_s . TIF is then utilized for calculating the motion flow
 410 of the query coordinate. Based on these outputs, we ob-
 411 tain the space-time feature by warping the continuous fea-
 412 ture domain. The wrapped feature at x_s corresponds to the
 413 continuous feature at x'_s . The relationship between two co-
 414 ordinates can be written as
 415

$$416 \quad 417 \quad x'_s = x_s + \mathcal{M}(x_s, x_t) \quad (5)$$

418 where $\mathcal{M}(x_s, x_t)$ is the motion flow vector at (x_s, x_t) .
 419

420 We query this new spatial coordinate in the continuous
 421 2D feature domain and obtain a new feature vector (the light
 422 green cuboid in Fig 2), which is treated as the feature of our
 423 continuous space-time representation at coordinate (x_s, x_t) .
 424 Accordingly, the continuous space-time feature \mathcal{F}_{st} can be
 425 formulated as
 426

$$427 \quad 428 \quad \mathcal{F}_{st}(x_s, x_t) = \mathcal{F}_s(x'_s) = \mathcal{F}_s(x_s + \mathcal{M}(x_s, x_t)) \quad (6)$$

429 3.4. Feature Decoding

430 Based on the continuous space-time representation, we
 431 can get the feature corresponding to any space-time coor-
 432 dinate. The final step is to decode the feature as an RGB
 433 value. A straightforward design is to take the obtained
 434 space-time feature for decoding directly. However, due to
 435

432 the MLP-based network architecture, the RGB value of every predicted pixel depends on a single feature vector, leading
433 to a limited size of the network receptive field. To alleviate the negative impact of this disadvantage, we enrich
434 the input information of the decoding network by aggregating
435 features of different scales. In detail, we incorporate
436 the encoded feature as well as two input frames for decoding.
437 Since these additional features are typically of low-
438 resolution compared with the target resolution, we sample
439 feature vectors corresponding to the query coordinate by bi-
440 linear interpolation. All features are then combined together
441 for predicting the RGB output.

442 3.5. Frame synthesis

443 From Section 3.1 to 3.4, we focus on predicting the RGB
444 value at a specific coordinate. To synthesize an entire frame,
445 we need to query coordinates of all pixels in it. Given these
446 coordinates, we can convert the continuous feature from SIF
447 into a high-resolution feature map. We can also generate a
448 complete motion flow field for the latent high-resolution
449 interpolated frame. Therefore, we do not have to forward SIF
450 twice before and after warping as in the situation of one
451 input coordinate. Instead, we warp the whole high-resolution
452 feature map based on the motion flow and input the warped
453 feature into the decoding network to synthesize the target
454 frame at one time.

455 4. Experiments

456 4.1. Experimental Setup

457 **Dataset.** We use Adobe240 dataset [41] as the training set,
458 which includes 133 videos in 720P taken by hand-held cameras.
459 We follow [48] to split these videos into the train, validation,
460 and test subsets with 100, 16, and 17 videos. All
461 videos are converted into image sequences for training and
462 testing. Each sequence contains approximately 3000 frames
463 which are treated as high-resolution frames in training. The
464 low-resolution counterparts are then generated by imresize
465 function in Matlab with the default setting of bicubic
466 interpolation. We use a sliding window to select frames from
467 the image sequences for training. The length of the sliding
468 window is set to 9. We take the 1st and 9th frames as network
469 inputs. The 2nd to 7th frames serve as ground-truth frames,
470 and we randomly select three of them as the supervision
471 of our network in every iteration. STIF is trained by two
472 stages. In the first stage, we fixed the down-sampling space
473 scale to $\times 4$. In the second stage, we randomly sample scales
474 in a uniform distribution $\mathcal{U}(1, 4)$. We provide more discussion
475 about this two-stage training strategy in Section 4.3.

476 Datasets including Vid4 [23], Adobe240 [41], and Go-
477 Pro [29] are used for evaluation. On Vid4, we only conduct
478 experiments on single frame interpolation of STVSR. For
479 Adobe240 and GoPro, we evaluate on their test set. The im-

480 age sequences extracted from videos in the datasets are split
481 into groups of 9-frame video clips. We feed the 1st and 9th
482 frames down-sampled by scale $\times 4$ in each clip into models
483 to generate 9 high-resolution frames from 1st to 9th. We
484 separately evaluate the average metrics of the *center* frames
485 (*i.e.* the 1st, 4th, 9th frames) and all 9 output frames. They
486 are denoted as *-Center* and *-Average* in Table 1.

487 **Implementation details.** We use Adam optimizer [22] with
488 $\beta_1 = 0.9$ and $\beta_2=0.999$. The learning rate is initialized as
489 1×10^{-4} and is decayed to 1×10^{-7} with a cosine annealing
490 for every 150,000 iterations. The model is trained in a total
491 of 600,000 iterations with batch size 24. The first training
492 stage includes 450,000 iterations while the second stage in-
493 cludes 150,000 iterations. The input frames in one batch
494 are down-sampled by the same space scale and randomly
495 cropped into patches with size 32×32 . We perform data
496 augmentation by randomly rotating 90° , 180° and 270° ,
497 and horizontal-flipping. We use Zooming SlowMo [47] as
498 the encoder. For the spatial implicit function and temporal
499 implicit function, we utilize two 3-layer SIRENs [39] with
500 hidden dimensions of [64, 64, 256]. For the decoding net-
501 work, we employ a 4-layer SIREN with hidden dimensions
502 of [64, 64, 256, 256]. As suggested in [47, 48], we select the
503 Charbonnier loss function for optimization.

504 **Evaluation.** Peak-Signal-to-Noise Ratio (PSNR) and
505 Structural Similarity Index (SSIM) [46] are employed to
506 evaluate model performances. We also compare the model
507 size and inference time to measure the efficiency of models.

510 4.2. Comparison to State-of-the-arts

511 We compare the proposed STIF with state-of-the-art
512 two-stage and one-stage STVSR methods. For two-stage
513 methods, we employ SuperSloMo [18], QVI [49], and
514 DAIN [2] for video frame interpolation (VFI); Bicubic
515 Interpolation, EDVR [45], and BasicVSR [6] for video
516 super-resolution (VSR). For one-stage methods, we com-
517 pare STIF with recently developed Zooming SlowMo [47]
518 and TMNet [48]. To perform fair comparisons, we train the
519 three VFI methods and Zooming SlowMo from scratch on
520 Adobe240 dataset. For TMNet, as mentioned in the original
521 paper that a two-stage training scheme is needed for conver-
522 gence, we pre-train the model on Vimeo90K [50] dataset
523 and fine-tune it on Adobe240 dataset [41]. Therefore, TM-
524 Net is trained on more data compared with other methods,
525 which may lead to some advantages in the comparison. To
526 compare with Zooming SlowMo that only supports fixed
527 frame interpolation, we train a new version of STIF named
528 STIF-*fixed* of which the interpolation time is fixed to 0.5.
529 **Quantitative results.** We present in-distribution quantita-
530 tive comparisons between STIF and other STVSR meth-
531 ods in Table 1. On single frame interpolation of STVSR
532 including Vid4, GoPro-*Center*, and Adobe-*Center*, STIF-
533 *Fixed* achieves competitive performance compared with

540 Table 1. **Quantitative comparison on benchmark datasets** including Vid4 [23], GoPro [29] and Adobe240 [41]. The best three results
 541 are highlighted in red, blue, and bold. We omit the results of Zooming SlowMo and STIF-Fixed on GoPro-Average and Adobe240-Average
 542 as the two models are trained for synthesizing frames only at fixed times.
 543

VFI Method	SR Method	Vid4		GoPro-Center		GoPro-Average		Adobe-Center		Adobe-Average		Parameters (Million)
		PSNR	SSIM	PSNR	SSIM	PSNR	SSIM	PSNR	SSIM	PSNR	SSIM	
SuperSloMo [18]	Bicubic	22.42	0.5645	27.04	0.7937	26.06	0.7720	26.09	0.7435	25.29	0.7279	19.8
SuperSloMo [18]	EDVR [45]	23.01	0.6136	28.24	0.8322	26.30	0.7960	27.25	0.7972	25.95	0.7682	19.8+20.7
SuperSloMo [18]	BasicVSR [6]	23.17	0.6159	28.23	0.8308	26.36	0.7977	27.28	0.7961	25.94	0.7679	19.8+6.3
QVI [18]	Bicubic	22.11	0.5498	26.50	0.7791	25.41	0.7554	25.57	0.7324	24.72	0.7114	29.2
QVI [18]	EDVR [45]	23.60	0.6471	27.43	0.8081	25.55	0.7739	26.40	0.7692	25.09	0.7406	29.2+20.7
QVI [18]	BasicVSR [6]	23.15	0.6428	27.44	0.8070	26.27	0.7955	26.43	0.7682	25.20	0.7421	29.2+6.3
DAIN [2]	Bicubic	22.57	0.5732	26.92	0.7911	26.11	0.7740	26.01	0.7461	25.40	0.7321	24.0
DAIN [2]	EDVR [45]	23.48	0.6547	28.01	0.8239	26.37	0.7964	27.06	0.7895	26.01	0.7703	24.0+20.7
DAIN [2]	BasicVSR [6]	23.43	0.6514	28.00	0.8227	26.46	0.7966	27.07	0.7890	26.23	0.7725	24.0+6.3
Zooming SlowMo [47]		25.72	0.7717	30.69	0.8847	-	-	30.26	0.8821	-	-	11.10
TMNet [48]		25.96	0.7803	30.14	0.8692	28.83	0.8514	29.41	0.8524	28.30	0.8354	12.26
STIF-fixed		25.78	0.7730	30.73	0.8850	-	-	30.21	0.8805	-	-	11.31
STIF		25.61	0.7709	30.26	0.8792	29.41	0.8669	29.92	0.8746	29.27	0.8651	11.31

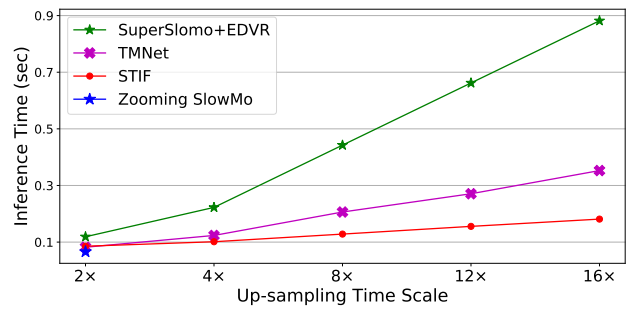
557 Table 2. **Quantitative comparison for out-of-distribution scales** on GoPro dataset. Model performances are evaluated by PSNR and
 558 SSIM. Some results of TMNet are bolded as it does not support generalizing to out-of-training-distribution space scales.
 559

Time Scale	Space Scale	SuperSloMo [18] + LIIF [7]	DAIN [2] + LIIF [7]	TMNet [48]	STIF
×6	×4	26.70 / 0.7988	26.71 / 0.7998	30.49 / 0.8861	30.78 / 0.8954
×6	×6	23.47 / 0.6931	23.36 / 0.6902	-	25.56 / 0.7671
×6	×12	21.92 / 0.6495	22.01 / 0.6499	-	24.02 / 0.6900
×12	×4	25.07 / 0.7491	25.14 / 0.7497	26.38 / 0.7931	27.32 / 0.8141
×12	×6	22.91 / 0.6783	22.92 / 0.6785	-	24.68 / 0.7358
×12	×12	21.61 / 0.6457	21.78 / 0.6473	-	23.70 / 0.6830
×16	×4	24.42 / 0.7296	24.20 / 0.7244	24.72 / 0.7526	25.81 / 0.7739
×16	×6	23.28 / 0.6883	22.80 / 0.6722	-	23.86 / 0.7123
×16	×12	21.80 / 0.6481	22.22 / 0.6420	-	22.88 / 0.6659

571 Table 3. **Quantitative comparison of out-of-distribution performance between STIF and the baseline Zooming SloMo model [47].** Evaluated on GOPRO dataset. -×A×B refers to A
 572 up-sampling space scale and B up-sampling time scale.
 573

Method	GoPro - ×4×2		GoPro - ×16×4	
	PSNR	SSIM	PSNR	SSIM
Zooming Slomo	30.69	0.8847	23.38	0.6708
STIF	30.26	0.8792	23.45	0.6710

582 other state-of-the-art models, while the performance of
 583 STIF slightly suffers. We attribute this observation to the
 584 difference of training targets between STIF and STIF-Fixed.
 585 The training settings of STIF-Fixed aim for synthesizing
 586 frames at pre-defined times. Therefore, it only learns fixed
 587 patterns between input frames instead of learning a con-
 588 tinuous representation as STIF does, leading to advantages in
 589 performances. On Vid4, TMNet performs the best, and we
 590 assume this is because TMNet is trained with more data as
 591 we noted in Section 4.2. For multiple frame interpolation
 592 of STVSR including GoPro-Average and Adobe-Average,
 593 STIF achieves the best performance, which indicates that



594 Figure 3. **Inference time of STVSR methods on different up-
 595 sampling time scales.** Note that We only select the most efficient
 596 two-stage method (SuperSlomo + EDVR) for comparison.
 597

598 the proposed implicit neural representation provides ad-
 599 vances on modeling the temporal information in videos.
 600

601 In Table 2, we present comparisons of STVSR meth-
 602 ods on out-of-distribution space and time scales. For two-
 603 stage STVSR methods, we select SuperSloMo and DAIN as
 604 VFI methods, and LIIF as the SR method since it can per-
 605 form super-resolution on arbitrary up-sampling scales. We
 606 also take TMNet into the comparison as it could general-
 607

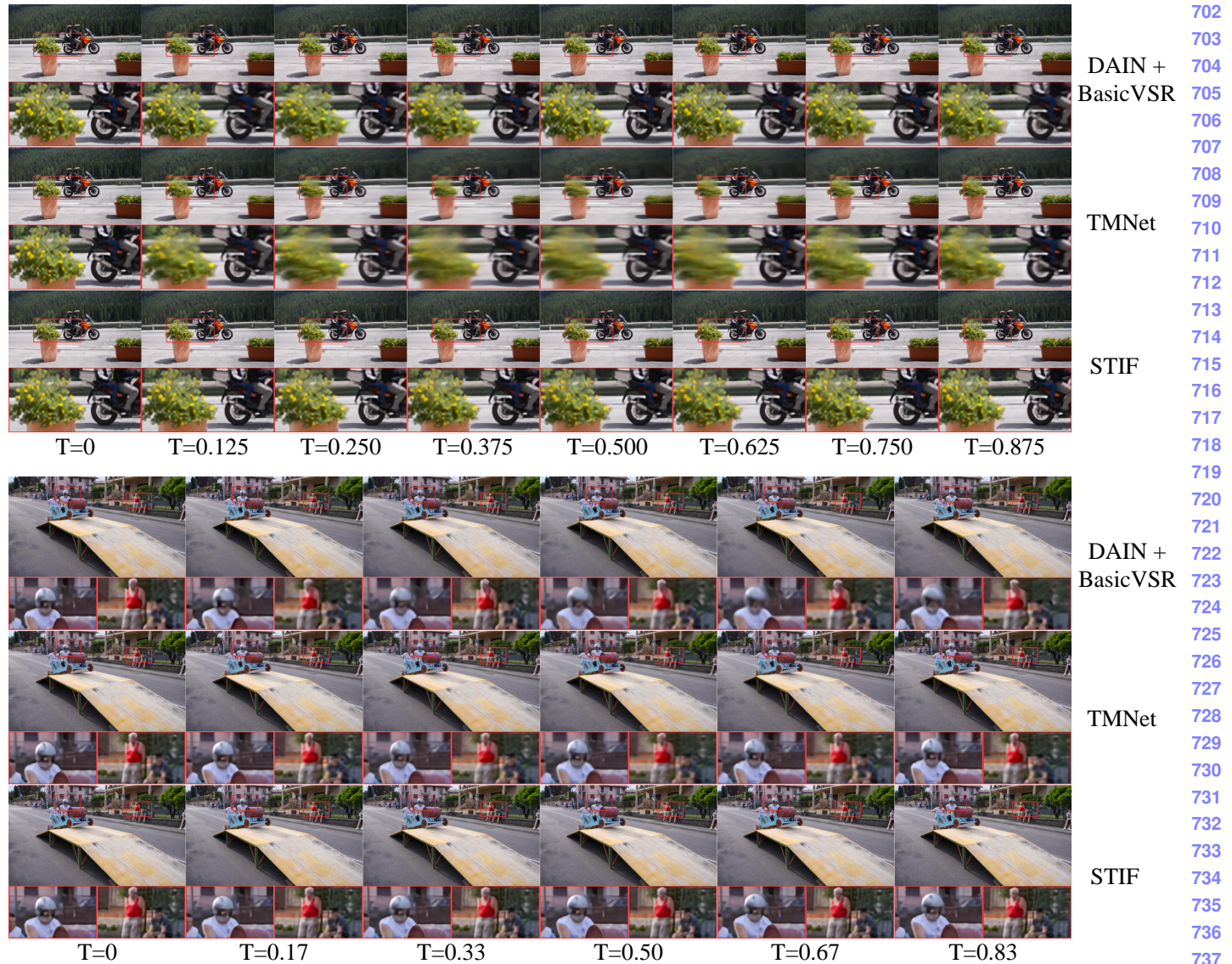


Figure 4. **Qualitative comparisons of different STVSR methods on arbitrary frame interpolation.** The interpolation times of the first example are in the training distribution and the times of the second example are out-of-distribution. Best zoom in for better visualization.

ize on time scales. We produce experiments on GoPro [29] dataset. We observe that STIF outperforms other methods by a large margin, demonstrating the advantage of our continuous video representation in out-of-distribution generalization. In addition, we further compare STIF with Zooming SlowMo (the encoder for STIF) in out-of-distribution scales. As Zooming SlowMo only supports interpolating fixed frames, we apply the model twice to achieve out-of-distribution inferences. In Table 3, we observe that while Zooming SlowMo performs slightly better on single frame interpolation ($\times 4 \times 2$), STIF achieves better performance in out-of-distribution testing ($\times 16 \times 4$).

We compare the inference time of STVSR methods in Figure 3. We observe that the efficiency of STIF is close to Zooming-SlowMo and TMNet at up-sampling time scale

$\times 2$, and STIF inferences faster than other models on multi-frame interpolation. We attribute this feature to the design of STIF, where all the latent frames between two input frames can be synthesized by MLPs after encoding.

Qualitative Results We demonstrate a qualitative comparison in Figure 4. We compare STIF with two STVSR methods, DAIN + BasicVSR and TMNet. The selected temporal coordinates of the first sample are in the training distribution, while the coordinates of the second sample are out-of-distribution. We find that the performance of DAIN + BasicVSR degrades in out-of-distribution circumstances (see the rider’s head in the second sample). TMNet fails to recover objects with large motion between two input frames (see the flowers in the first sample). The performance of STIF is steady across both in-distribution and out-of-

756 Table 4. **Ablation study on architecture designs of STIF.** Evaluated on GOPRO and Adobe240 dataset. -f/m refers to removing flow
 757 correspondence and multi-scale feature aggregation. -s refers to decoding both time and space by a single implicit function. 810
 758 811
 759 812
 760 813
 761 814
 762 815
 763 816
 764 817
 765 818
 766 819
 767 820
 768 821

Architecture Design	GoPro-Center		GoPro-Average		Adobe-Center		Adobe-Average	
	PSNR	SSIM	PSNR	SSIM	PSNR	SSIM	PSNR	SSIM
STIF	30.26	0.8792	29.41	0.8669	29.92	0.8746	29.27	0.8651
STIF (-f)	29.63	0.8719	28.76	0.8614	29.19	0.8641	28.50	0.8569
STIF (-m)	29.99	0.8751	29.28	0.8655	29.68	0.8690	29.04	0.8606
STIF (-s)	29.86	0.8741	29.20	0.8654	29.42	0.8678	28.95	0.8613

765 Table 5. **Ablation study on STIF trained with different data settings.** Evaluated on GOPRO-Average. - $\times 4$ refers to fixing the down-
 766 sampling space scale to $\times 4$ throughout the training. *-continuous* refers to training STIF by continuous space scales from scratch. 820
 767 821

Training Settings	Space $\times 2$		Space $\times 3$		Space $\times 4$		Space $\times 6$		Space $\times 12$	
	PSNR	SSIM	PSNR	SSIM	PSNR	SSIM	PSNR	SSIM	PSNR	SSIM
STIF	29.61	0.8734	29.14	0.8685	29.41	0.8669	25.40	0.7590	24.11	0.6913
STIF (- $\times 4$)	28.25	0.8490	28.62	0.8626	29.50	0.8696	25.24	0.7567	23.82	0.6857
STIF (<i>-continuous</i>)	27.46	0.8268	28.35	0.8507	28.82	0.8541	25.10	0.7533	23.62	0.6801

775 distribution temporal coordinates, indicating that learning
 776 continuous video representations helps to improve model
 777 generalization in STVSR task.

4.3. Ablation Study

780 **Motion Flow Field.** Motion flow is one critical component
 781 of STIF. Previous video interpolation methods [16, 18] have
 782 already demonstrated that such a learnable flow helps to inter-
 783polate frames with sharp edges and clear details. We propose
 784 that the motion flow field brings two main advantages.
 785 First, the flow field could capture non-local information and
 786 temporal contexts of large motions. Second, we explicitly
 787 apply spatial warping on features, which works as an in-
 788 ductive bias for the training. In Table 4 between STIF and
 789 STIF (-f), we show that the performance degrades when the
 790 motion flow is not incorporated in STIF.

791 **STIF trained with different data settings.** In Table 5, we
 792 compare the performances of STIF trained on different data
 793 settings. As noted before, STIF follows a two-stage training
 794 strategy: fixed down-sampling space scale for the first stage
 795 and continuous space scales sampled from a uniform dis-
 796 tribution for the second stage. STIF- $\times 4$ indicates that the
 797 space scale is fixed to $\times 4$ throughout the training of STIF.
 798 STIF-*continuous* represents STIF trained with continuous
 799 down-sampling space scales from scratch. We find that the
 800 performance suffers a significant drop when we train STIF
 801 only on continuous scales. We hypothesize this is because
 802 the network needs to learn spatial and temporal represen-
 803 tations at the same time, and it becomes extremely difficult to
 804 learn such temporal representation when the scale of spa-
 805 tial features keeps varying. Besides, we observe that train-
 806 ing STIF with a fixed space scale achieves slightly better
 807 performance for that specific scale. However, its general-
 808 ization performance is competed by STIF trained by two
 809 stages, which is demonstrated by the comparisons between

828 STIF and STIF (- $\times 4$) on space scales other than $\times 4$. 829

830 **Other design choices.** We provide more ablation studies in
 831 Table 4. By comparing STIF with STIF (-m), we find that
 832 the proposed multi-scale feature aggregation contributes to
 833 performance improvement. We also try to combine SIF and
 834 TIF into a single implicit function, that is, we use one im-
 835 plicit function to generate the continuous motion flow and
 836 apply spatial warping only on the encoded feature and input
 837 frames. The results between STIF and STIF (-s) indicate
 838 that using two implicit functions for representing space and
 839 time outperforms only one implicit function for them all. 840

5. Discussion

841 **Conclusion.** In this paper, we present a Space-Time Im-
 842 plicit Function (STIF) for continuous video representa-
 843 tion. STIF can represent videos in arbitrary spatial and
 844 temporal resolution, which brings natural advantages for
 845 solving space-time video super-resolution (STVSR) tasks.
 846 Extensive experiments show that STIF performs compet-
 847 itively with state-of-the-art STVSR methods on common
 848 up-sampling scales and outperforms prior works by a large
 849 margin on out-of-distribution scales. 850

851 **Limitations and Future Work.** We observe that there exist
 852 few cases for which STIF does not perform very well. These
 853 cases typically need to handle very large motions, which is
 854 still an open challenge for video interpolation. 855

856 **Ethical Concerns.** STIF interpolates frames based on
 857 learned statistics of the training dataset. Thus, it would re-
 858 flect biases in those data, including ones with negative soci-
 859 etal impacts. STIF may generate nonexistent or fake contents.
 860 These issues warrant further consideration before process-
 861 ing videos by STIF. As researchers, we are committed to
 862 against misconduct behaviors and pursue research that is to
 863 the benefit of society. 864

864
865
866
867
868
869
870
871
872
873
874
875
876
877
878
879
880
881
882
883
884
885
886
887
888
889
890
891
892
893
894
895
896
897
898
899
900
901
902
903
904
905
906
907
908
909
910
911
912
913
914
915
916
917

References

- [1] Ivan Anokhin, Kirill Demochkin, Taras Khakhulin, Gleb Sterkin, Victor Lempitsky, and Denis Korzenkov. Image generators with conditionally-independent pixel synthesis. In *Proceedings of the IEEE/CVF Conference on Computer Vision and Pattern Recognition*, pages 14278–14287, 2021. [2](#)
- [2] Wenbo Bao, Wei-Sheng Lai, Chao Ma, Xiaoyun Zhang, Zhiyong Gao, and Ming-Hsuan Yang. Depth-aware video frame interpolation. In *Proceedings of the IEEE/CVF Conference on Computer Vision and Pattern Recognition*, pages 3703–3712, 2019. [2, 5, 6](#)
- [3] Jose Caballero, Christian Ledig, Andrew Aitken, Alejandro Acosta, Johannes Totz, Zehan Wang, and Wenzhe Shi. Real-time video super-resolution with spatio-temporal networks and motion compensation. In *Proceedings of the IEEE/CVF Conference on Computer Vision and Pattern Recognition*, pages 4778–4787, 2017. [2](#)
- [4] Joao Carreira and Andrew Zisserman. Quo vadis, action recognition? a new model and the kinetics dataset. In *proceedings of the IEEE Conference on Computer Vision and Pattern Recognition*, pages 6299–6308, 2017. [1](#)
- [5] Eric R Chan, Marco Monteiro, Petr Kellnhofer, Jiajun Wu, and Gordon Wetzstein. pi-gan: Periodic implicit generative adversarial networks for 3d-aware image synthesis. In *Proceedings of the IEEE/CVF Conference on Computer Vision and Pattern Recognition*, pages 5799–5809, 2021. [2](#)
- [6] Kelvin CK Chan, Xintao Wang, Ke Yu, Chao Dong, and Chen Change Loy. Basicvsr: The search for essential components in video super-resolution and beyond. In *Proceedings of the IEEE/CVF Conference on Computer Vision and Pattern Recognition*, pages 4947–4956, 2021. [2, 5, 6](#)
- [7] Yinbo Chen, Sifei Liu, and Xiaolong Wang. Learning continuous image representation with local implicit image function. In *Proceedings of the IEEE/CVF Conference on Computer Vision and Pattern Recognition*, pages 8628–8638, 2021. [2, 4, 6](#)
- [8] Zhiqin Chen and Hao Zhang. Learning implicit fields for generative shape modeling. In *Proceedings of the IEEE/CVF Conference on Computer Vision and Pattern Recognition (CVPR)*, June 2019. [2](#)
- [9] Jifeng Dai, Haozhi Qi, Yuwen Xiong, Yi Li, Guodong Zhang, Han Hu, and Yichen Wei. Deformable convolutional networks. In *Proceedings of the IEEE/CVF Conference on Computer Vision and Pattern Recognition*, pages 764–773, 2017. [2](#)
- [10] Boyang Deng, John P Lewis, Timothy Jeruzalski, Gerard Pons-Moll, Geoffrey Hinton, Mohammad Norouzi, and Andrea Tagliasacchi. Nasa neural articulated shape approximation. In *Computer Vision–ECCV 2020: 16th European Conference, Glasgow, UK, August 23–28, 2020, Proceedings, Part VII 16*, pages 612–628. Springer, 2020. [2](#)
- [11] Terrance DeVries, Miguel Angel Bautista, Nitish Srivastava, Graham W Taylor, and Joshua M Susskind. Unconstrained scene generation with locally conditioned radiance fields. *arXiv preprint arXiv:2104.00670*, 2021. [2](#)
- [12] Christoph Feichtenhofer, Haoqi Fan, Jitendra Malik, and Kaiming He. Slowfast networks for video recognition. In *Proceedings of the IEEE/CVF international conference on computer vision*, pages 6202–6211, 2019. [1](#)
- [13] Kyle Genova, Forrester Cole, Avneesh Sud, Aaron Sarna, and Thomas Funkhouser. Local deep implicit functions for 3d shape. In *Proceedings of the IEEE/CVF Conference on Computer Vision and Pattern Recognition*, pages 4857–4866, 2020. [2](#)
- [14] Kyle Genova, Forrester Cole, Daniel Vlasic, Aaron Sarna, William T Freeman, and Thomas Funkhouser. Learning shape templates with structured implicit functions. In *Proceedings of the IEEE/CVF International Conference on Computer Vision*, pages 7154–7164, 2019. [2](#)
- [15] Muhammad Haris, Greg Shakhnarovich, and Norimichi Ukita. Space-time-aware multi-resolution video enhancement. In *Proceedings of the IEEE/CVF Conference on Computer Vision and Pattern Recognition*, pages 2859–2868, 2020. [1, 3](#)
- [16] Zhewei Huang, Tianyuan Zhang, Wen Heng, Boxin Shi, and Shuchang Zhou. Rife: Real-time intermediate flow estimation for video frame interpolation. *arXiv preprint arXiv:2011.06294*, 2020. [8](#)
- [17] Takashi Isobe, Xu Jia, Shuhang Gu, Songjiang Li, Shengjin Wang, and Qi Tian. Video super-resolution with recurrent structure-detail network. In *European Conference on Computer Vision*, pages 645–660. Springer, 2020. [2](#)
- [18] Huaiyu Jiang, Deqing Sun, Varun Jampani, Ming-Hsuan Yang, Erik Learned-Miller, and Jan Kautz. Super slomo: High quality estimation of multiple intermediate frames for video interpolation. In *Proceedings of the IEEE/CVF Conference on Computer Vision and Pattern Recognition*, pages 9000–9008, 2018. [2, 5, 6, 8](#)
- [19] Younghyun Jo, Seoung Wug Oh, Jaeyeon Kang, and Seon Joo Kim. Deep video super-resolution network using dynamic upsampling filters without explicit motion compensation. In *Proceedings of the IEEE/CVF Conference on Computer Vision and Pattern Recognition*, pages 3224–3232, 2018. [2](#)
- [20] Tero Karras, Miika Aittala, Samuli Laine, Erik Härkönen, Janne Hellsten, Jaakko Lehtinen, and Timo Aila. Alias-free generative adversarial networks. *arXiv preprint arXiv:2106.12423*, 2021. [2](#)
- [21] Soo Ye Kim, Jihyong Oh, and Munchurl Kim. Fisr: deep joint frame interpolation and super-resolution with a multi-scale temporal loss. In *Proceedings of the AAAI Conference on Artificial Intelligence*, volume 34, pages 11278–11286, 2020. [1, 3](#)
- [22] Diederik P Kingma and Jimmy Ba. Adam: A method for stochastic optimization. *arXiv preprint arXiv:1412.6980*, 2014. [5](#)
- [23] Ce Liu and Deqing Sun. A bayesian approach to adaptive video super resolution. In *Proceedings of the IEEE/CVF Conference on Computer Vision and Pattern Recognition*, pages 209–216. IEEE, 2011. [2, 5, 6](#)
- [24] Lars Mescheder, Michael Oechsle, Michael Niemeyer, Sebastian Nowozin, and Andreas Geiger. Occupancy networks:

- 972 Learning 3d reconstruction in function space. In *Proceedings* 1026
973 of the IEEE/CVF Conference on Computer Vision and Pattern 1027
974 Recognition (CVPR), June 2019. 2 1028
- 975 [25] Simone Meyer, Oliver Wang, Henning Zimmer, Max Grosse, 1029
976 and Alexander Sorkine-Hornung. Phase-based frame interpolation 1030
977 for video. In *Proceedings of the IEEE/CVF Conference on Computer 1031
978 Vision and Pattern Recognition*, pages 1410–1418, 2015. 2 1032
979
- 980 [26] Mateusz Michalkiewicz, Jhony K Pontes, Dominic Jack, 1033
981 Mahsa Baktashmotagh, and Anders Eriksson. Implicit 1034
982 surface representations as layers in neural networks. In *Proceedings 1035
983 of the IEEE/CVF International Conference on Computer Vision*, 1036
984 pages 4743–4752, 2019. 2 1037
- 985 [27] Ben Mildenhall, Pratul P Srinivasan, Matthew Tancik, 1038
986 Jonathan T Barron, Ravi Ramamoorthi, and Ren Ng. Nerf: 1039
987 Representing scenes as neural radiance fields for view synthesis. 1040
988 In *European conference on computer vision*, pages 405–421. Springer, 2020. 2 1041
- 989 [28] Uma Mudenagudi, Subhashis Banerjee, and Prem Kumar 1042
990 Kalra. Space-time super-resolution using graph-cut optimization. 1043
991 *IEEE Transactions on Pattern Analysis and Machine 1044
992 Intelligence*, 33(5):995–1008, 2010. 1, 3 1045
- 993 [29] Seungjun Nah, Tae Hyun Kim, and Kyoung Mu Lee. Deep 1046
994 multi-scale convolutional neural network for dynamic scene 1047
995 deblurring. In *Proceedings of the IEEE/CVF Conference 1048
996 on Computer Vision and Pattern Recognition*, pages 3883– 1049
997 3891, 2017. 2, 5, 6, 7 1050
- 998 [30] Simon Niklaus and Feng Liu. Context-aware synthesis for 1051
999 video frame interpolation. In *Proceedings of the IEEE/CVF 1052
1000 Conference on Computer Vision and Pattern Recognition*, 1053
1001 pages 1701–1710, 2018. 2 1054
- 1002 [31] Simon Niklaus and Feng Liu. Softmax splatting for video 1055
1003 frame interpolation. In *Proceedings of the IEEE/CVF Conference 1056
1004 on Computer Vision and Pattern Recognition*, pages 5437–5446, 2020. 2 1057
- 1005 [32] Simon Niklaus, Long Mai, and Feng Liu. Video frame 1058
1006 interpolation via adaptive convolution. In *Proceedings of the 1059
1007 IEEE/CVF Conference on Computer Vision and Pattern 1060
1008 Recognition*, pages 670–679, 2017. 2 1061
- 1009 [33] Simon Niklaus, Long Mai, and Feng Liu. Video frame 1062
1010 interpolation via adaptive separable convolution. In *Proceedings 1063
1011 of the IEEE International Conference on Computer Vision*, 1064
1012 pages 261–270, 2017. 2 1065
- 1013 [34] Jeong Joon Park, Peter Florence, Julian Straub, Richard 1066
1014 Newcombe, and Steven Lovegrove. Deepsdf: Learning 1067
1015 continuous signed distance functions for shape representation. 1068
1016 In *Proceedings of the IEEE/CVF Conference on Computer 1069
1017 Vision and Pattern Recognition (CVPR)*, June 2019. 2 1070
- 1018 [35] Fitsum A Reda, Deqing Sun, Aysegul Dundar, Mohammad 1071
1019 Shoeybi, Guilin Liu, Kevin J Shih, Andrew Tao, Jan Kautz, 1072
1020 and Bryan Catanzaro. Unsupervised video interpolation using 1073
1021 cycle consistency. In *Proceedings of the IEEE/CVF International 1074
1022 Conference on Computer Vision*, pages 892–900, 2019. 2 1075
- 1023 [36] Katja Schwarz, Yiyi Liao, Michael Niemeyer, and Andreas 1076
1024 Geiger. Graf: Generative radiance fields for 3d-aware image 1077
1025 synthesis. *arXiv preprint arXiv:2007.02442*, 2020. 2 1078
- 1026 [37] Oded Shahar, Alon Faktor, and Michal Irani. *Space-time 1079
1027 super-resolution from a single video*. IEEE, 2011. 1, 3
1028 [38] Eli Shechtman, Yaron Caspi, and Michal Irani. Increasing 1029
1029 space-time resolution in video. In *European Conference on 1030
1030 Computer Vision*, pages 753–768. Springer, 2002. 1, 3
1031 [39] Vincent Sitzmann, Julien Martel, Alexander Bergman, David 1032
1032 Lindell, and Gordon Wetzstein. Implicit neural representations 1033
1033 with periodic activation functions. *Advances in Neural 1034
1034 Information Processing Systems*, 33, 2020. 5
1035 [40] Ivan Skorokhodov, Savva Ignatyev, and Mohamed Elhosseiny. 1036
1036 Adversarial generation of continuous images. In *Proceedings 1037
1037 of the IEEE/CVF Conference on Computer Vision and Pattern 1038
1038 Recognition*, pages 10753–10764, 2021. 2
1039 [41] Shuochen Su, Mauricio Delbracio, Jue Wang, Guillermo 1040
1040 Sapiro, Wolfgang Heidrich, and Oliver Wang. Deep video 1041
1041 deblurring for hand-held cameras. In *Proceedings of the 1042
1042 IEEE/CVF Conference on Computer Vision and Pattern 1043
1043 Recognition*, pages 1279–1288, 2017. 2, 5, 6
1044 [42] Deqing Sun, Xiaodong Yang, Ming-Yu Liu, and Jan Kautz. 1045
1045 Pwc-net: Cnns for optical flow using pyramid, warping, and 1046
1046 cost volume. In *Proceedings of the IEEE/CVF Conference 1047
1047 on Computer Vision and Pattern Recognition*, pages 8934– 1048
1048 8943, 2018. 2
1049 [43] Xin Tao, Hongyun Gao, Renjie Liao, Jue Wang, and Ji- 1050
1049 aya Jia. Detail-revealing deep video super-resolution. In *Proceedings 1051
1050 of the IEEE/CVF International Conference on Computer 1051
1051 Vision*, pages 4472–4480, 2017. 2
1052 [44] Yapeng Tian, Yulun Zhang, Yun Fu, and Chenliang Xu. 1053
1053 Tdan: Temporally-deformable alignment network for video 1054
1054 super-resolution. In *Proceedings of the IEEE/CVF Conference 1055
1055 on Computer Vision and Pattern Recognition*, pages 3360–3369, 2020. 2
1056 [45] Xintao Wang, Kelvin CK Chan, Ke Yu, Chao Dong, and 1057
1057 Chen Change Loy. Edvr: Video restoration with enhanced 1058
1058 deformable convolutional networks. In *Proceedings of the 1059
1059 IEEE/CVF Conference on Computer Vision and Pattern 1060
1060 Recognition Workshops*, pages 0–0, 2019. 2, 5, 6
1061 [46] Zhou Wang, Alan C Bovik, Hamid R Sheikh, and Eero P Si- 1062
1062 moncelli. Image quality assessment: from error visibility to 1063
1063 structural similarity. *IEEE transactions on image processing*, 1064
1064 13(4):600–612, 2004. 5
1065 [47] Xiaoyu Xiang, Yapeng Tian, Yulun Zhang, Yun Fu, Jan P 1066
1066 Allebach, and Chenliang Xu. Zooming slow-mo: Fast and 1067
1067 accurate one-stage space-time video super-resolution. In *Proceedings 1068
1068 of the IEEE/CVF conference on computer vision and pattern 1069
1069 recognition*, pages 3370–3379, 2020. 1, 3, 5, 6
1070 [48] Gang Xu, Jun Xu, Zhen Li, Liang Wang, Xing Sun, and 1071
1071 Ming-Ming Cheng. Temporal modulation network for 1072
1072 controllable space-time video super-resolution. In *Proceedings 1073
1073 of the IEEE/CVF Conference on Computer Vision and 1074
1074 Pattern Recognition*, pages 6388–6397, 2021. 1, 3, 5, 6
1075 [49] Xiangyu Xu, Li Siyao, Wenxiu Sun, Qian Yin, and Ming- 1076
1076 Hsuan Yang. Quadratic video interpolation. *Advances 1077
1077 in Neural Information Processing Systems*, 32:1647–1656, 1078
1078 2019. 2, 5
1079

- 1080 [50] Tianfan Xue, Baian Chen, Jiajun Wu, Donglai Wei, and 1134
1081 William T Freeman. Video enhancement with task- 1135
1082 oriented flow. *International Journal of Computer Vision*, 1136
1083 127(8):1106–1125, 2019. 2, 5 1137
- 1084 [51] Xizhou Zhu, Han Hu, Stephen Lin, and Jifeng Dai. De- 1138
1085 formable convnets v2: More deformable, better results. In 1139
1086 *Proceedings of the IEEE/CVF Conference on Computer Vi- 1140
1087 sion and Pattern Recognition*, pages 9308–9316, 2019. 2 1141
- 1088 [52] Xizhou Zhu, Yujie Wang, Jifeng Dai, Lu Yuan, and Yichen 1142
1089 Wei. Flow-guided feature aggregation for video object detec- 1143
1090 tion. In *Proceedings of the IEEE International Conference on 1144
1091 Computer Vision*, pages 408–417, 2017. 1 1145
- 1092 1146
- 1093 1147
- 1094 1148
- 1095 1149
- 1096 1150
- 1097 1151
- 1098 1152
- 1099 1153
- 1100 1154
- 1101 1155
- 1102 1156
- 1103 1157
- 1104 1158
- 1105 1159
- 1106 1160
- 1107 1161
- 1108 1162
- 1109 1163
- 1110 1164
- 1111 1165
- 1112 1166
- 1113 1167
- 1114 1168
- 1115 1169
- 1116 1170
- 1117 1171
- 1118 1172
- 1119 1173
- 1120 1174
- 1121 1175
- 1122 1176
- 1123 1177
- 1124 1178
- 1125 1179
- 1126 1180
- 1127 1181
- 1128 1182
- 1129 1183
- 1130 1184
- 1131 1185
- 1132 1186
- 1133 1187